Contact Force Models, including Electric Contact Deformation, for Electrostatically Actuated, Cantilever-Style, RF MEMS Switches

R. A. Coutu, Jr.* and P. E. Kladitis*

* Air Force Institute of Technology
AFIT/ENG 2950 Hobson Way, Wright Patterson AFB, OH, USA
ronald.coutu@afit.edu, ronald.coutu@wpafb.af.mil, paul.kladitis@afit.edu

ABSTRACT

Electrostatically actuated, cantilever-style, metal contact, radio frequency (RF), microelectromechanical systems (MEMS) switches depend on having adequate contact force to achieve desired, low contact resistance. In this study, contact force equations that account for beam tip deflection and electric contact material deformation are derived. Tip deflection is modeled analytically using beam bending theory and contact material deformation is modeled as elastic, plastic, or elastic-plastic. Contact resistance predictions, based on Maxwellian theory and newly derived contact force equations, are compared to experimental results. Contact force predictions not considering tip deflection or material deformation overestimate contact force and result in underestimated contact resistance. Predictions based on the new contact force models agree with measurements.

Keywords: microelectromechanical systems, micro-switch, contact force, contact resistance

1 INTRODUCTION

This paper reports on contact force models for electrostatically actuated, cantilever-style, radio frequency (RF), microelectromechanical systems (MEMS) metal contact switches like that shown in Figure 1.

This new contact force modeling approach considers beam tip deflection and electric contact material deformation that occurs after switch closure. Prior studies focused on mechanical designs to achieve the high contact force needed for low contact resistance connections [1]. The effects of tip deflection and material deformation on contact force in electrostatically actuated, micro-switches has not been addressed. Previous work by this author, showed that contact force, bounded by pull-in and collapse voltages, could be analytically modeled using the beam illustrated in Figure 2 [2].

Equation 1 is the resulting contact force equation [3]:

$$F_{\mathrm{c}} = \frac{F_{\mathrm{a}}}{2l^3} a^2 (3l - a) \tag{1}$$

**The views expressed in this article are those of the authors and do not reflect the official policy or position of the United States Air Force, Department of Defense, or the U.S. Government.

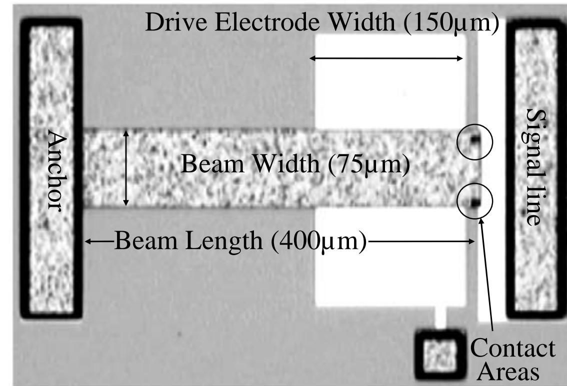

Figure 1: A captured video image of a 75 μm-wide by 400 μm-long micro-switch.

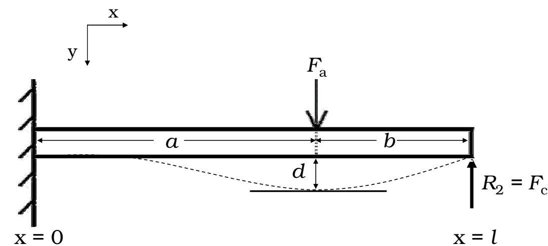

Figure 2: Cantilever beam model with a fixed end at $x = 0$, a simply supported end at $x = l$, and an intermediately placed external load (F_{a}) at $x = a$.

where F_{c} is contact force (μN), F_{a} is applied electrostatic force (μN), a is the location of the applied electrostatic force (μm), and l is beam length (μm). This simple model does not consider either beam tip deflection or contact material deformation after switch closure or pull-in.

In this study, contact force equations are derived by assuming elastic, plastic, and elastic-plastic electric contact material deformation [4] and modeling tip deflection [3]. Beam bending equations, material deformation models, and the principle of superposition are used to derive the new contact force equations.

2 IMPROVED SWITCH MODEL

In metal contact micro-switches, initial switch closure is defined by the pull-in voltage. At pull-in, physical contact between the switch's upper and lower electric contacts is first established, with minimal contact force. Increased actuation voltage causes higher contact force and increased pressure at the surface asperities resulting in contact material deformation.

After pull-in, the switch is best modeled as a deflected beam with a fixed end, a simply supported end, an intermediate external load (F_a), and contact material deformation, as illustrated in Figure 3.

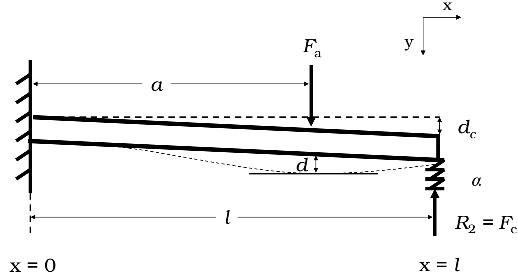

Figure 3: Deflected cantilever beam model with a fixed end at $x = 0$, a simply supported end at $x = l$, an intermediately placed external load (F_a) at $x = a$ and contact material deformation (α) at $x = l$.

The external load (F_a), modeled as electrostatic force, was found by neglecting fringing fields and using a first-order parallel plate capacitor description:

$$F_a = \frac{\epsilon_o A_{sa} V^2}{2g^2} \tag{2}$$

where ϵ_o is dielectric permittivity ($\frac{F}{\mu m}$), A_{sa} is surface area (μm^2) of one plate, V is applied voltage (V), and g is the gap (μm) under the beam.

Like Figure 2, the beam in Figure 3 is statically indeterminate and another equation is needed to supplement the static equilibrium equations (i.e. $\sum F_x = 0, \sum F_y = 0$, and $\sum M = 0$). Using superposition, tip deflection is represented by the sum of two statically determinate systems. The first is a beam with a fixed end, a free end, and an intermediate load (F_a) and the second is a beam with a fixed end, a free end, and an end load ($-R_2$).

Using the method of moments, Equation 3 results for the maximum tip deflection for the first statically determinate system (beam with intermediate load) [3]:

$$d = \frac{F_a a^2}{6EI_z}(3l - a) \tag{3}$$

where d is maximum cantilever beam tip deflection (μm), E is elastic modulus (GPa), and I_z is the area moment of inertia about the z-axis ($\frac{m^4}{12}$). The method of moments is also used to determine Equation 4 or the maximum tip deflection for the second statically determinate system (beam with end load) [3]:

$$d' = \frac{-R_2 l^3}{3EI_z} \tag{4}$$

where d' is maximum cantilever beam tip deflection (μm).

The final equation, needed to solve the indeterminate system in Figure 3, is found by summing Equations 3 and 4, setting that sum equal to overall tip deflection (i.e. the sum of the distance between the electric contacts and the amount of material deformation), and solving for the reaction force, R_2, results in:

$$R_2 = [\frac{F_a a^2}{2l^3}(3l - a)] - [\frac{3EI_z}{l^3}(d_c + \alpha)] \tag{5}$$

where d_c is the gap between the electric contacts (μm) and α is contact material vertical deformation (μm). In micro-switches, the beam reaction force (R_2) is equal to contact force and the external load is equal to electrostatic force. Substituting F_c for R_2, Equation 2 for F_a, and $g = g_o - d$, in Equation 5 results in:

$$F_c = [\frac{\epsilon_o A_{sa} V^2}{4l^3(g_o - d)^2} a^2 (3l - a)] - [\frac{3EI_z}{l^3}(d_c + \alpha)]. \tag{6}$$

3 MATERIAL DEFORMATION

Contact force is a compressive force that causes material deformation similar to that predicted by conventional material tensile testing. The difference being tensile loads cause material deformation by necking out and compressive loads cause deformation by bulging. Elastic, plastic, and elastic-plastic material deformation models are discussed next.

3.1 Elastic

When electric contact surfaces initially come together, they experience elastic or reversible material deformation. Equations 7 and 8 define the contact area and force as a function of vertical deformation [4]:

$$A = \pi R \alpha \tag{7}$$

where A is contact area (μm^2), R is radius of curvature (μm), and α is vertical deformation (μm) and

$$F_c = \frac{4}{3} E' \alpha \sqrt{R\alpha} \tag{8}$$

where F_c is contact force (μN) and E' is Hertzian modulus (GPa) defined by:

$$\frac{1}{E'} = \frac{1 - \nu_1^2}{E_1} + \frac{1 - \nu_2^2}{E_2} \tag{9}$$

where E_1 is elastic modulus (GPa) and ν_1 is Poisson's ratio for contact one and E_2 and ν_2 are for contact two. For circular areas (i.e. $A = \pi r^2$), Equations 7 and 8 are related to the effective contact area radius (r_{eff}) (μm) through Hertz's contact radius model [5]:

$$r_{\text{eff}} = \sqrt[3]{\frac{3F_c R}{4E'}}. \tag{10}$$

Vertical deformation, in terms of contact force, is derived when $A = \pi r_{\text{eff}}^2$ is substituted into Equation 7, solved for R, and then substituted into Equation 10, resulting in:

$$\alpha = (\frac{3F_{\text{c}}}{4E' r_{\text{eff}}}). \tag{11}$$

When deformation is no longer reversible and the material has gone passed the yield point (Y), plastic deformation begins. Fully plastic deformation, discussed next, occurs when the contact load exceeds $\sim 3Y$ [5].

3.2 Plastic

Plastic material deformation is modeled using the well known fully plastic contact model [6]. Equations 12 and 13 define the contact area and force as a function of vertical deformation [4]:

$$A = 2\pi R\alpha \tag{12}$$

and

$$F_{\text{c}} = HA \tag{13}$$

where H (GPa) is the Meyer hardness [5]. Vertical deformation, in terms of contact force, results when Equation 12 is substituted into Equation 13 and solved for α, resulting in:

$$\alpha = \frac{F_{\text{c}}}{2\pi HR}. \tag{14}$$

When using the elastic model from section 3.1 and this plastic model, an area discontinuity exists during the transition from elastic to fully plastic behavior [5]. Chang addressed this by assuming volume conservation of deformed asperities and developing an elastic-plastic material deformation model suitable from initial plasticity onset to fully plastic behavior [4].

3.3 Elastic-Plastic

Elastic-plastic material deformation refers to the situation when portions of the contact area are plastically deformed but completely surrounded by elastic material. This phase of material deformation occurs beyond the elastic limit but prior to fully plastic behavior. Equation 15 is used to define the critical vertical asperity deformation limit where initial elastic-plastic material deformation begins [4]:

$$\alpha_{\text{c}} = R(\frac{H\pi}{2E'})^2 \tag{15}$$

where α_{c} is critical vertical deformation (μm). Equations 16 and 17 are the contact area and force equations from Chang's elastic-plastic model [4]:

$$A = \pi R\alpha(2 - \frac{\alpha_{\text{c}}}{\alpha}) \tag{16}$$

and

$$F_{\text{c}} = [3 + (\frac{2}{3}K_{\text{Y}} - 3)\frac{\alpha_{\text{c}}}{\alpha}]YA \tag{17}$$

where K_{Y} is the yield coefficient given by Equation 18:

$$K_{\text{Y}} = 1.282 + 1.158\nu. \tag{18}$$

Since most metals exhibit a yield point equal to one third the material's hardness ($\frac{H}{3}$) and a yield coefficient (K_{Y}) approximately equal to three [4], Equation 17 can be rewritten as:

$$F_{\text{c}} = [1 - (\frac{\alpha_{\text{c}}}{3\alpha})]HA. \tag{19}$$

Vertical deformation, in terms of contact force, is derived when $A = \pi r_{\text{eff}}^2$ is substituted into Equation 19 and then solved for α, resulting in Equation 20:

$$\alpha = \frac{1}{3}(\frac{H\pi r_{\text{eff}}^2 \alpha_c}{H\pi r_{\text{eff}}^2 - F_{\text{c}}}). \tag{20}$$

New contact force models are derived next using the above material deformation models.

4 NEW CONTACT FORCE MODELS

When contact areas deform elastically, a contact force model is derived by substituting Equation 11 into Equation 6 resulting in:

$$F_{\text{cE}} = [\frac{\epsilon_{\text{o}} A_{\text{sa}} V^2}{4l^3(g_{\text{o}} - d)^2} a^2(3l - a)] - [\frac{3EI_{\text{z}}}{l^3}(d_{\text{c}} + \frac{3F_{cE}}{4E' r_{\text{eff}}})]. \tag{21}$$

Solving Equation 21 for F_{cE} results in:

$$\boxed{F_{\text{cE}} = 2E' r_{\text{eff}}[\frac{(\frac{\epsilon_{\text{o}} A_{\text{sa}} V^2}{2(g_{\text{o}} - d)^2})a^2(3l - a) - (6E' I_{\text{z}} d_{\text{c}})}{(9EI_{\text{z}} + 4E' r_{\text{eff}} l^3)}]}. \tag{22}$$

For plastically deforming contact areas a contact force model is derived by substituting Equation 14 into Equation 6 resulting in:

$$F_{\text{cP}} = [\frac{\epsilon_{\text{o}} A_{\text{sa}} V^2}{4l^3(g_{\text{o}} - d)^2} a^2(3l - a)] - [\frac{3EI_{\text{z}}}{l^3}(d_{\text{c}} + \frac{F_{\text{cP}}}{2\pi HR})]. \tag{23}$$

Solving Equation 23 for F_{cP} results in:

$$\boxed{F_{\mathrm{cP}} = \pi H R [\frac{(\frac{\epsilon_{\mathrm{o}} A_{\mathrm{sa}} V^2}{2(g_{\mathrm{o}}-d)^2}) a^2 (3l-a) - (6EI_{\mathrm{z}} d_{\mathrm{c}})}{(3EI_{\mathrm{z}} + 2\pi H R l^3)}]}. \tag{24}$$

For elastic-plastic deformation, a contact force model is derived by substituting Equation 20 into Equation 6 resulting in:

$$\begin{aligned} F_{\mathrm{cEP}} &= [\frac{\epsilon_{\mathrm{o}} A_{\mathrm{sa}} V^2}{4l^3 (g_{\mathrm{o}} - d)^2} a^2 (3l - a)] - \\ & [\frac{3EI_{\mathrm{z}}}{l^3} (d_{\mathrm{c}} + \frac{1}{3} (\frac{H \pi r_{\mathrm{eff}}^2 \alpha_{\mathrm{c}}}{H \pi r_{\mathrm{eff}}^2 - F_{\mathrm{cEP}}})]. \end{aligned} \tag{25}$$

Solving Equation 25 for F_{cEP} results in:

$$\boxed{F_{\mathrm{cEP}}^2 + C_1 F_{\mathrm{cEP}} = C_2} \tag{26}$$

where

$$\boxed{C_1 = \frac{1}{2l^3} [(6EI_{\mathrm{z}} d_{\mathrm{c}}) - (2\pi H l^3 r_{\mathrm{eff}}^2) - (\frac{\epsilon_{\mathrm{o}} A_{\mathrm{sa}} V^2}{2(g_{\mathrm{o}} - d)^2}) a^2 (3l - a)]}$$

and

$$\boxed{C_2 = \frac{H \pi r_{\mathrm{eff}}^2}{2l^3} [2EI_{\mathrm{z}} (3d_{\mathrm{c}} + \alpha_{\mathrm{c}}) - (\frac{\epsilon_{\mathrm{o}} A_{\mathrm{sa}} V^2}{2(g_{\mathrm{o}} - d)^2}) a^2 (3l - a)]}.$$

5 RESULTS

The micro-switches shown in Figure 1 were designed, fabricated, and tested. The electroplated gold structural layer was $\sim 5\ \mu m$-thick and the gold-on-gold electric contacts consisted of two hemispherical upper contacts $\sim 8\ \mu m$ in diameter ($\sim 3\ \mu m$ radius of curvature) and a flat lower contact. The elastic modulus, hardness, and resistivity used in the analytic predictions were 80 GPa, 2 GPa, and 2 $\mu\Omega - cm$, respectively [5]. An Alessi Rel-4100A probe station, HP 6181B DC voltage source and HP 3455A digital voltmeter were used to actuate the switches with $\sim 60\ V_{\mathrm{DC}}$ and measure the contact resistance using a four-point probe configuration.

Contact resistance measurements and predictions, based on Maxwellian spreading resistance theory [5], elastic, plastic, and elastic-plastic contact material deformation [4], and the new, improved contact force models (Equations 22, 24, and 26) are summarized in Table 1 for devices with three different drive electrode widths.

Note from Table 1, the elastic-plastic based predictions agree best with the measurements. This indicates that the contact surface asperities were deformed beyond the elastic limit and material deformation was best characterized using an elastic-plastic model [4].

Contact resistance, in terms of the new contact force model (Equation 26) and the original contact force model (Equation 1), are compared in Table 2. Note that contact resistance predictions, as a function of the new contact force model agree with measurements better than predictions based on the original contact force model. Also from Table 2, note that contact force (per contact) found using Equation 1 (F_{c}) is substantially higher than that found using Equation 26 (F_{cEP}).

Table 1: Contact resistance measurements and analytic predictions for switches with varying drive electrode widths, contact materials with elastic, plastic, and elastic-plastic material deformations, and the new, improved contact force models (Equations 22, 24, and 26).

Width	Measured R_{c}	R_{cE}	R_{cP}	R_{cEP}
50 μm	0.353 Ω	0.089 Ω	0.179 Ω	0.189 Ω
100 μm	0.253 Ω	0.067 Ω	0.111 Ω	0.123 Ω
150 μm	0.263 Ω	0.056 Ω	0.085 Ω	0.096 Ω

Table 2: Contact resistance predictions for switches with varying drive electrode widths. The contact force values were found using a new contact force model (Equation 26) and the original contact force model (Equation 1).

Width	$R_{\mathrm{cEP}}(F_{\mathrm{cEP}})$	F_{cEP}	$R_{\mathrm{cEP}}(F_{\mathrm{c}})$	F_{c}
50 μm	0.189 Ω	2.95 μN	0.121 Ω	7.13 μN
100 μm	0.123 Ω	6.89 μN	0.084 Ω	15.00 μN
150 μm	0.096 Ω	11.32 μN	0.066 Ω	23.86 μN

6 CONCLUSIONS

Contact force models not accounting for beam tip deflection and material deformation (Equation 1) overestimate micro-switch contact force. Measurement and prediction discrepancies, normally attributed to contaminant film resistance, result when contact force is overestimated. The new micro-switch contact force models contain both mechanical beam parameters and contact material properties that are important for evaluating switch designs and selecting contact materials.

REFERENCES

[1] D. Peroulis, et al., IEEE MTT, 51, 259–70, 2003.

[2] R. Coutu, Jr., et al., Proceedings: Eurosensors XVII, Guimarães, Portugal, 64–67, 2003.

[3] J. Shigley and C. Mischke, "Mech. Engineering Design, 5th Ed.," McGraw-Hill, New York, 1990.

[4] W. Chang, J. of Wear, 212, 229–27, 1997.

[5] R. Holm, "Electric Contacts: Theory and Applications," Berlin: Springer, 1969.

[6] E. Abbot and F. Firestone, ASME, 55, 569, 1933.